AFRL-OSR-VA-TR-2015-0087

STRUCTURED NANOWIRES FOR SPECTRA-TUNED AND SPECTRA-MULTIPLEXED SENSING THZ GENER

Jimmy Xu
BROWN UNIVERSITY IN PROVIDENCE IN STATE OF RI AND PROVIDENCE PLANTATIONS

04/08/2015
Final Report

Air Force Research Laboratory
AF Office Of Scientific Research (AFOSR)/ RTD
Arlington, Virginia 22203
Air Force Materiel Command

REPORT DOCUMENTATION PAGE

Form Approved
OMB No. 0704-0188

PLEASE DO NOT RETURN YOUR FORM TO THE ABOVE ORGANIZATION.

1. REPORT DATE *(DD-MM-YYYY)*	2. REPORT TYPE	3. DATES COVERED *(From - To)*
03-03-2015	Final report	04/15/10 - 04/14-15

4. TITLE AND SUBTITLE
"Structured Nanowires for Spectra-Tuned and Spectra-Multiplexed Sensing THZ Generation"

5a. CONTRACT NUMBER

5b. GRANT NUMBER
FA9550-10-0109

5c. PROGRAM ELEMENT NUMBER

6. AUTHOR(S)
Professor Jimmy Xu

5d. PROJECT NUMBER

5e. TASK NUMBER

5f. WORK UNIT NUMBER

7. PERFORMING ORGANIZATION NAME(S) AND ADDRESS(ES)
Brown University
Office of the Sponsored Projects
Box 1929, 164 Angell Street,
Providence, RI 02912-9002

8. PERFORMING ORGANIZATION REPORT NUMBER

9. SPONSORING/MONITORING AGENCY NAME(S) AND ADDRESS(ES)
Adaptive Sensing and GHz-THz-Speed Electronics
AF Office of Scientific Research
875 N. Randolph St.
Arlington, VA 22203
(703)588-0194

10. SPONSOR/MONITOR'S ACRONYM(S)

11. SPONSOR/MONITOR'S REPORT NUMBER(S)

12. DISTRIBUTION/AVAILABILITY STATEMENT

13. SUPPLEMENTARY NOTES

14. ABSTRACT

15. SUBJECT TERMS

16. SECURITY CLASSIFICATION OF:			17. LIMITATION OF ABSTRACT	18. NUMBER OF PAGES	19a. NAME OF RESPONSIBLE PERSON
a. REPORT	b. ABSTRACT	c. THIS PAGE			19b. TELEPHONE NUMBER *(Include area code)*

The Final Report

Title: Structured Nanowires for Spectra-Tuned and Spectra-Multiplexed Sensing THz Generation

Principal Investigator:
Jimmy Xu, Ph.D., Professor, Brown University

Telephone: +1-401-863-1439
E-mail: Jimmy_Xu@brown.edu

Contract Number: FA9550-10-1-0109

AFOSR Program Manager: Dr. Kitt C. Reinhardt

Period of Performance: 5 year

Submission Date: Apr. 8th, 2015

Table of contents

1. Objectives:

The purpose of this project was to:

1. develop a new class of nanoelectronic nanostructures (e.g. nanowire and nanowire network structures) made of materials whose electronic properties are dependent of size in the nano regime. An example of such a material is bismuth, which can be tuned from metallic to semiconducting at room temperature and, even more dramatically, from superconducting to insulating at cryogenic temperatures, by controlled variation of one physical dimension in the size regime of 50 nm and below,
2. demonstrate the feasibility of tuning along the length of the conduction path and thereby varying the spectral range of the sensing response of the chosen segment,
3. demonstrate the formation of a built-in metallic terminal at the end by increasing the conduction path dimension to the extent (> 50 nm) when it is larger than its Fermi wavelength,
4. fabricate and investigate a novel three-port nanowire structures,

5. conduct research into the steady state spectroscopic characteristics of the fabricated structures and their dependences on the diameter modulation, the base materials, the contact conditions, and the growth and surface conditions, and
6. in the case of a three-port nanowire structure, e.g. a T-junction, test and investigate strategies and implementation of designs for real-time spectral tuning through the third port,
7. in addition to the proposed technology developments and demonstrations, address and establish a good understanding of a number of basic scientific issues arising from the electron transport across the unique quantum mechanical systems of the diameter-modulated and three-terminal nanowires as well as the growth mechanisms.

2. Overview and achievements:

1. The performance of nanowire (NW)-based electrical devices can be significantly affected by electrical contacts between electrodes and NWs, sometimes to the extent that it is really the contacts that determine the performance. We reported [1] that the conventional methods for contact evaluation can give rise to considerable errors because of an altered property of the NW under the electrodes.
2. One-dimensional (1D) bismuth and bismuth sulfide nanowires have been successfully fabricated. The diameter of bismuth nanowires was precisely controlled from 66 to 25 nm using atomic layer deposition (ALD) and IR absorption characteristics were investigated [2]. Discovery of an environmentally friendly new sulfur source molecule critical for metal sulfide synthesis; we introduced a new sulfur source molecule for synthesis of high-aspect ratio and single-crystalline nanowires of bismuth sulfide in a low-temperature, solvothermal reaction process without a template [3].
3. In a theoretical study we reported [4] on the geometry-and size-dependent effects of metal-semiconductor contacts to understand the origins of significant contact effects on nanowire (NW) devices. The study suggests that the formation of a higher doping concentration in the contact regions is essential for better NW transistors.
4. Step-shaped bismuth (Bi) nanowires were fabricated by direct current electrochemical deposition technique using diameter-modulated anodic aluminum oxide membranes (AAO) as templates. We observed transition of nanowire property from semimetal to semiconductor at wire diameter below 50 nm [5].
5. The mechanism of the photoconductive gains of nanowires (NW) was not well understood. To this end, we demonstrated [6] that the photoconductive gain of a Bi2S3 NW photodetector can be contributed to by optical modulation of the electrical injection through contacts. We proposed a quantitative model to explain the results based on a model of metal-nanowire contacts.
6. Three-port T-junction bismuth-based nanowire structures were successfully synthesized, with transconductance modulation via a third-terminal control and tuning.
7. We investigated [7] quantum confinement effects in Bi anti-dot or 2-D diameter-modulated nanowire networks grown on anodized aluminum oxide templates. Magnetoresistance measurements revealed a well-defined weak anti-localization effect, one that is purely quantum mechanical in origin, below 10 K.
8. Due to the rich interplays of the unusually light effective mass of electrons (delocalization), high Fermi velocity, and superconductivity in bismuth, we thoroughly investigated the system of ultrathin (<10nm) Bi films patterned with a nanohoneycomb array of holes (or effectively hexagonal networks of bismuth nanowires). Most notably, we reported observations of unusual quantum phase-transitions in such system, starting with one which undergoes a thickness-tuned

insulator-superconductor transition that was cited by the American Institute of Physics in its year-end Bulletin as one of "Top-Ten Physics Stories" of the year and laid the foundation of the subsequent pursuits and successes in this project that have led to many publications (for example, [8-11])

9. At metal-insulator phase transitions a so-called "dielectric anomaly" is expected to occur, which has been reported in another material system in the THz range [12] and could in principle be tuned. To this end, we investigated thermally evaporated ultra-thin Bi films throughout the tunneling regime and the resulting percolation transition. In addition, we demonstrated that quantum effects are unlikely to be observed at room temperature in this regime.

3. Bi nanowires:

3.1 Introduction:

As a model system for 1D anisotropic material properties, Bismuth (Bi), in particular, is truly interesting. Bi is a semimetal with rhombohedral structure containing two atoms per unit cell. Due to the extraordinary large electron mean free path (~ 100 nm at room temperature and ~ 400 nm at 4.2K) and Fermi wavelength (~ 40 nm at room temperature), quantum-size effects are expected for Bi NWs with relatively large diameter [13-17]. The small electron effective masses (~ 0.001 m_0) and small overlap of valence and conduction bands (~ 38 meV at 77K) together with a low carrier density make Bi NW a promising material to show semimetal to semiconductor transition, high thermoelectric performance, and magnetoresistance even at relatively larger diameters (~ 50 nm) and at higher temperature than any other nanostructured materials [4, 18-22]. The change of conduction mechanism by reduced dimensionality is accompanied by yet another drastic change – the change of band gap and density of states with diameter.

Taking a larger perspective, Bismuth is one of the most interesting elemental materials on the periodic table, perhaps only second to Carbon in terms of the variety of distinctively different behaviors it can manifest. At room temperature it is a semimetal, but it could become semiconducting when it is confined in one or more dimensions to 50 nm or below due to its larger Fermi wavelength (~40 nm). At low temperature, it is a superconductor which has been known for a long time. What was not known and came as a complete surprise was that it could become an insulator, as we have recently found, with the AFOSR support to a prior project. We found that nano-scale periodic patterning of bismuth could induce a dramatic transition from superconducting to insulating due to localization of the Cooper pairs, (Science 2007, which was cited by American Institute of Physics in its year-end bulletin as one of the "Top Ten Physics News of 2007"). Bismuth [23-25] and bismuth-based compound semiconductors are also known for their superior thermoelectric power, rendering themselves for another mode of sensing in the far-infrared.

3.2 AAO fabrication method:

One nanowire fabrication method utilized extensively throughout this project was the technique of atomic layer deposition (ALD) into anodized alumina oxide (AAO) templates. Aluminum, when carefully anodized in an electrochemical bath, forms a tough oxide layer with a lattice of regularly spaced "pores" that go completely through the layer. These pores can then be filled using one of several methods with a variety of materials, forming nanowires. The nanowires can then be used in this

template (as discussed later), or the template can be dissolved, leaving the nanowires intact. This research leveraged a solid base with AFOSR support, in collaboration with a group at the Kookmin University, Korea.

Nanowire fabrication using AAO templates has many advantages over other methods. Fabrication of the nanopore array AAO templates can be done with precision modulation of the diameter at a given length along the pore. Diameter controlled fabrication of Bi nanowires has been demonstrated in the range of diameter between 60 nm and 36 nm in a collaborative effort between the two groups at Kookmin and Brown [2]. The pore length can also be tuned, as well as the pore spacing. Large numbers of nanowires can be produced at once, and contacted within the template, as well, which is an advantage over many other methods in which nanowires have to be contacted individually.

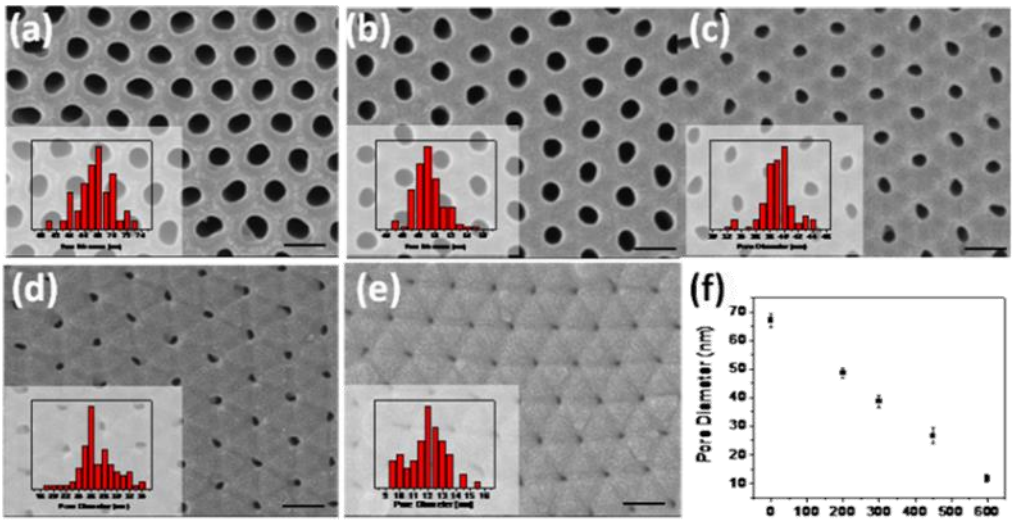

Figure 2 SEM image of precisely diameter-controlled porous alumina templates. The pore diameters are (a) 66±2.52 nm, (b) 48±1.86 nm, (c) 38±2.24 nm, (d) 25±2.48 nm, (e) 11±1.32 nm. (f) shows the graph of relationships between ALD cycles and pore diameters.

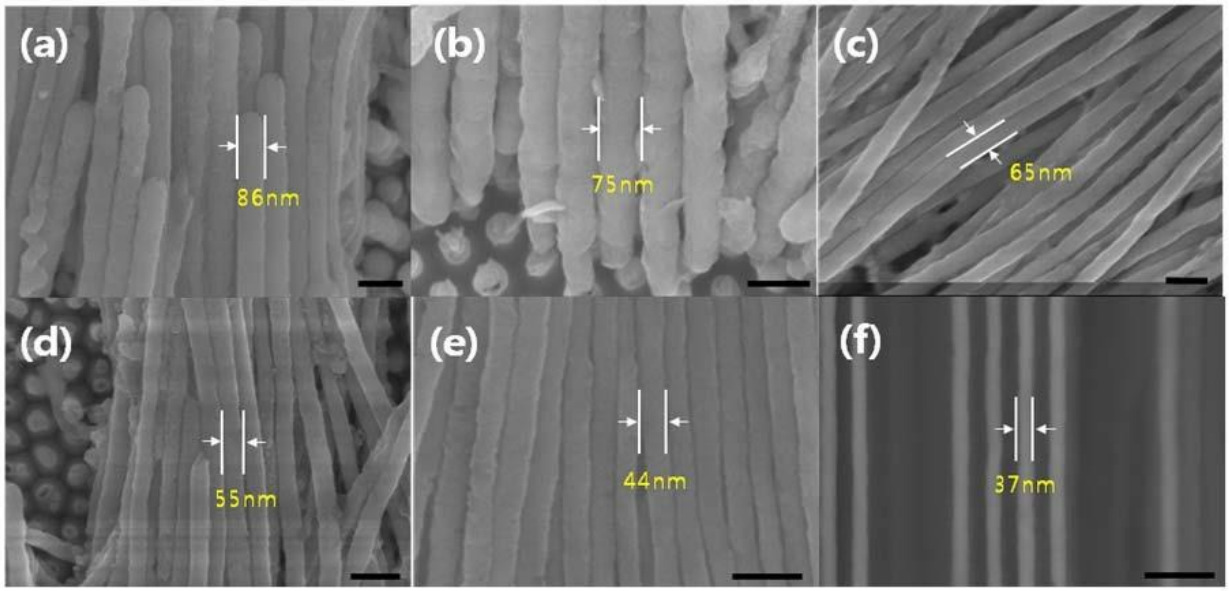

Figure 1 SEM image of Bi nanowires. (a) - (e) show the bundle of Bi nanowires without AAO template with various diameters. (f) shows the cross sectional image of Bi nanowires in AAO template. All scale bars are 100 nm.

The AAO template is fabricated by a well-known 2-step anodization method. The diameter of pores in AAO templates produced by a typical anodization process in our lab is around 70 nm. Then, the diameter of the AAO template pores is precisely reduced by conformally coating a thin oxide layer inside

pores using the ALD technique. The resulting pores as shown in Figure 1 with inner pore diameters and standard deviations in AAO templates are (a) 66±2.52 nm, (b) 48±1.86 nm, (c) 38±2.24 nm, (d) 25±2.48 nm, and (e) 11±1.32 nm. The pores are well ordered with a hexagonal arrangement and its standard deviations are less than ~ 10% of their diameters.

Following this, a layer of platinum (Pt) with the thickness of 200 nm is sputtered onto the one face of the ALD-coated AAO templates; this Pt layer will serve as an electrode during electrochemical deposition. After deposit of the Pt electrode, the AAO templates were attached to silicon wafer as a supporter. Chemically removing the backing Al metal gives the AAO templates the form of membranes. Additional etching is also carried out to remove the barrier layer on the bottom side of the AAO membranes. Surface treatment is also done on the inner pores of the membranes to make them hydrophilic. Bi nanowires are then deposited in a two electrode plating cell at room temperature. After electrochemical deposition of bismuth, the AAO template can be removed by chemical etching, without disruption of the Bi nanowires. Figure 2 (a)-(e) show fabricated Bi nanowires after removal of the AAO template.

3.3 OFF-ON fabrication method:

A novel method for producing Bi nanowires with high crystallinity was originally produced by [26, 27]. The gist of the method is that a Bi film is deposited by evaporation onto a glass substrate, which is then carefully manipulated by temperature. The Bi film and the substrate have different coefficients of heat expansion, which causes a stress on the Bi film. This in turn causes material flow such that atoms of Bi are pushed out away from the film in between the grain boundaries; the atoms that were previously pushed out in this fashion are pushed out farther by the next atoms pushed out, which forms a nanowire.

This slow, atom-by-atom fabrication method necessarily leads to nanowires of high crystallinity because it has the time to seek the lowest energy state while it is being built [28]. While highly crystalline AAO nanowires have been reported [29], they do not seem to be the norm; most tend to be composed of grains of different orientations. OFF-ON nanowires offer higher crystallinity and increased surface smoothness, as shown in figure 3.

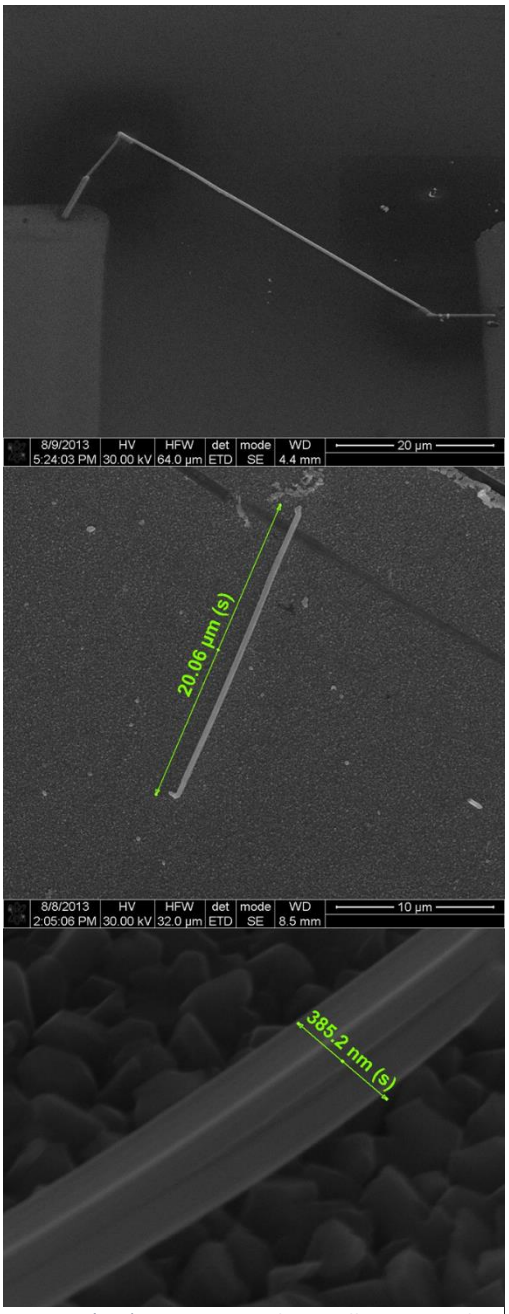

Figure 3 (top) OFF-ON NW electrically contacted using FIB deposition. (middle) Wide view of OFF-ON NW produced by this laboratory on fabrication substrate. (bottom) Close up of OFF-ON NW showing extreme surface smoothness.

3.4 E-beam lithography fabrication method:

Another fabrication method was employed to potentially fabricate high numbers of customized nanowires for spectral sensing, namely, electron beam lithography. In this method, a very thin layer of a chemical (or several), known as the “resist”, is spun onto a substrate. The resist can then be precisely

patterned with an electron beam using a Scanning Electron Microscope (SEM). Patterning in this context is simply exposing the regions to be patterned, which causes the resist to undergo a chemical change known as "crosslinking"; this is exactly analogous to analog photography. The crosslinking action is essentially when the polymer that comprises the resist is caused by the electron beam to connect to other polymers and become bigger, or break down into smaller polymers (depending on the type of resist), changing its solubility in another chemical known as the "developer".

This change in solubility allows one to expose arbitrary patterns, and then apply the developer such that it removes only the exposed patterns from the resist. From here, Bi is deposited over the whole substrate. After this deposition ("metallization"), the substrate is soaked in a strong solvent that removes the remaining resist (that didn't get exposed), along with the metal that has been deposited on top of it, leaving only the metal that was deposited directly onto the substrate (where the resist was originally exposed and developed/removed).

Because this process is entirely customizable, one can make highly novel and interesting structures, limited only by the physical limits of the SEM, the resist, and the metallization process (the electron beam can only be focused so narrowly; the resist gets exposed in a small area around where the beam hits; the metal is also deposited in finitely small chunks, so for a small enough feature size it will not successfully stick to the substrate). Nanowires have been formed in this manner down to at least 20 nm width [30].

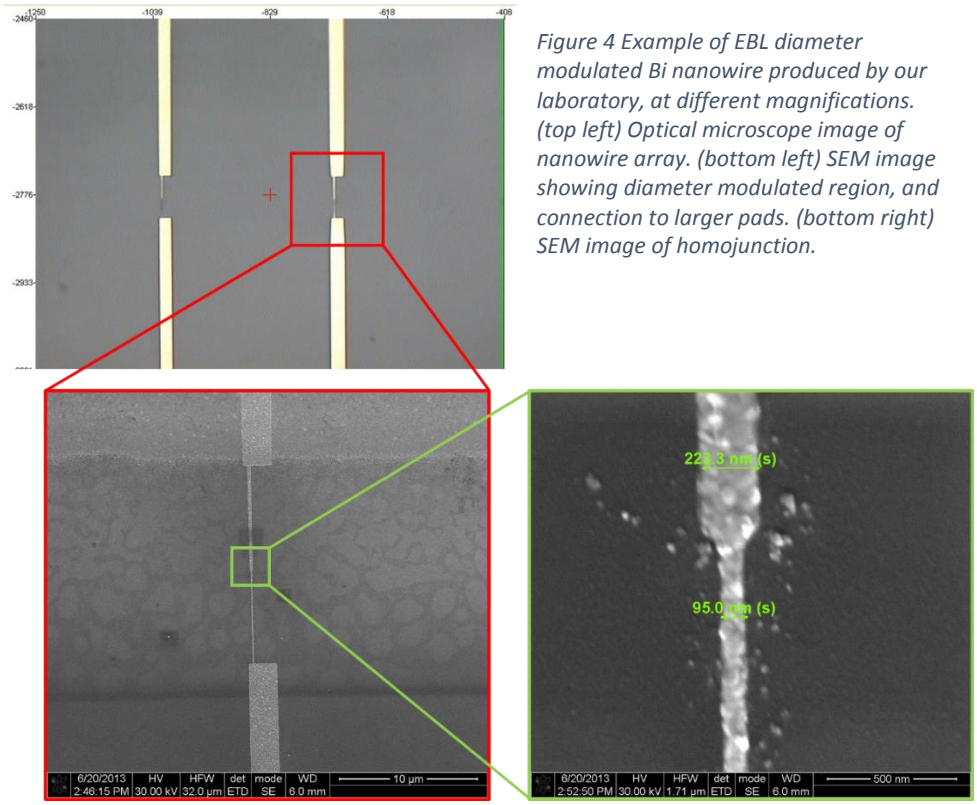

Figure 4 Example of EBL diameter modulated Bi nanowire produced by our laboratory, at different magnifications. (top left) Optical microscope image of nanowire array. (bottom left) SEM image showing diameter modulated region, and connection to larger pads. (bottom right) SEM image of homojunction.

This method is not without downsides (it requires a trained operator, it requires significant time for each batch, batch size is limited, and the wires will never have great crystallinity due to the deposition method), but its potential benefits outweighs these negatives for many applications. For example, as discussed in the following section, fabricating nanowires with diameter modulation is as trivial as making any shape. Thus, nano-antennas and nanowires can easily be customized to achieve the desired properties which are highly dependent on feature size. Additionally, while it is impossible to fabricate numbers of nanowires comparable to template-based methods such as AAO pore filling, it is very advantageous to be able to produce up to 10^3 nanowires that are already electrically contacted, because many methods of nanowire fabrication can produce high numbers (~10^5-10^7) of nanowires at once, but they have to be individually electrically contacted to characterize or use them. Thus, when attempting to do optical measurements, much more apparent signals are realized when using this higher number of nanowires enabled by e-beam lithography.

3.5 Diameter modulation:

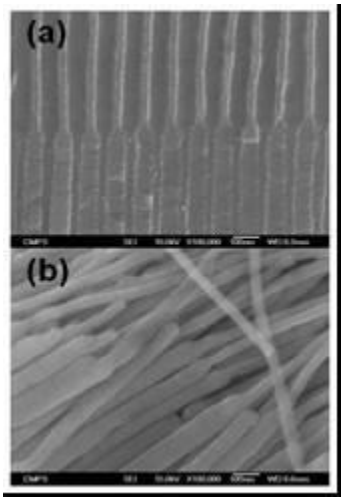

Figure 5 Diameter modulated AAO Bi nanowires. (a) Still in AAO template, (b) with template removed.

To accomplish the controlled nanowires' diameter modulation, we introduced programmed variation of the anodization voltage during the anodization of the high-purity aluminum film to form the desired aluminum oxide membrane with arrayed nanopores whose diameter is varied along the length to serve as the growth template. This technique is one with proven success in the range between 20 nm and 70 nm and has been used by the team, and many other groups now, to fabricate uniform nanowire and nanotube arrays, an example of which is shown in figure 5. Figure 5 also shows its cross-section view while still embedded in the aluminum oxide template. The figure clearly confirms that all nanowires have the same diameter which is abruptly changed to another value at the same length.

Step-shaped bismuth (Bi) nanowires were fabricated by direct current electrochemical deposition technique using diameter-modulated anodic aluminum oxide membranes (AAO) as templates. The nanowires have core-sheath structure with a crystalline rhombohedral Bi core surrounded by a mixed oxide (amorphous and monoclinic Bi_2O_3) layer.

I

n this work, controlled synthesis of step-shaped crystalline Bi NWs has been achieved. To our best knowledge, it is a first success in the formation of a nanowire with built-in metal-semiconductor self-homojunction.

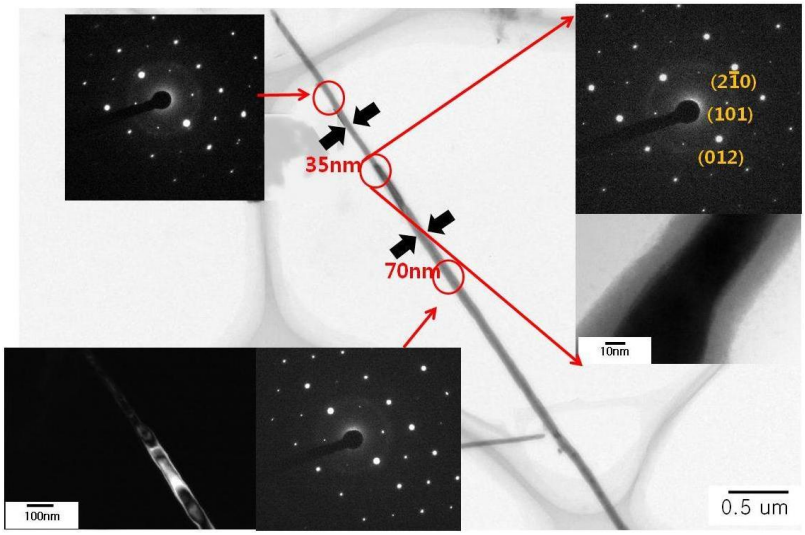

Figure 6 HRTEM study of step-shaped Bi nanowires (a) bright field images (b) SAED pattern corresponding to the neck region (c) SAED pattern corresponding to the broad region (d) SAED pattern corresponding to the step zone and magnified bright field image of the step zone.

3.5 Optical characteristics:

To determine whether the fabricated nanowires do possess the expected size-dependent semimetal to semiconductor transition, we measured IR abortion and reflection spectra for Bi nanowire array with various diameters. The measured nanowire arrays were embedded in the AAO growth templates. FTIR was used to obtain the absorption spectra in mid-IR range (i.e., 1.25 ~ 20 μm). The dimensions of the measured samples are summarized in the table I. As a control, sample 5 was prepared to measure IR absorption by pure AAO.

TABLE 1. Dimensions of Bi nanowires in AAO pores.

Sample number	Bi nanowire diameter (nm)	AAO template height (μm)	Bi nanowire length (μm)
3	38	9.6	6
4	50	9.8	7
5	-	9.8	-
8	67	12	5

Since the Bi/AAO structures are fabricated on 200 nm-thick Pt layer and IR source cannot transmit through the substrate, reflection spectra instead were measured for investigating IR absorption. Reflectance was calibrated by reflected mid-IR intensity from an Al mirror. We have checked that the bottom Pt electrode of Bi/AAO structure can be assumed as an ideal mirror by measuring reflected signals from an AAO template with the same metal film on top.

Figure 7 shows the measured reflection spectra for the Bi/AAO samples. All measured spectra are normalized by Al mirror reference spectrum (i). Flat reflectance of backside electrode implies a negligible effect of the bottom electrode and the substrate on IR absorption (ii). Periodic oscillation in the measured reflectance is indicative of interference within an unfilled portion of the transparent AAO template (AAO film effect) (iii). With sample 5 (iv), we obtained larger reflectance compared with (v), (vi) and (vii), which suggests IR absorption by Bi nanowires. Transition from high absorption to low absorption with decreasing diameter (v) indicates that the thinner (38 nm – diameter) Bi nanowires have turned into semiconducting and acquired a band gap. Plot vii shows high absorption over the MIR range, which indicates metallic Bi nanowire array is a good IR absorber. Decreased reflectance over 500 ~ 1800 cm^{-1} indicates lights with a wavelength of 5-20 μm are significantly absorbed by AAO (viii).

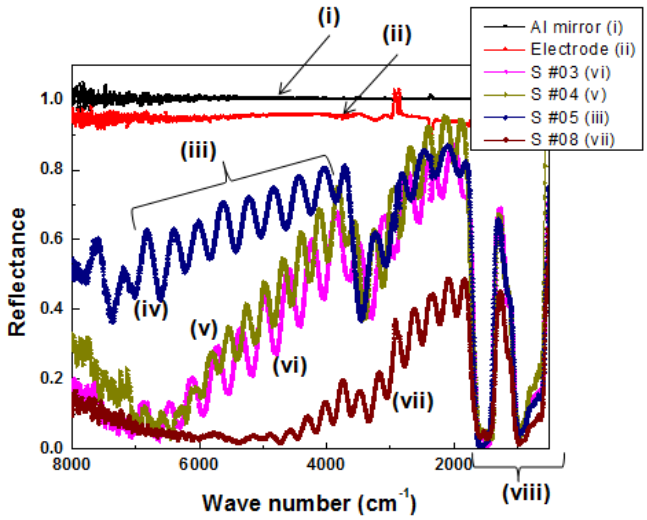

Figure 7 Reflectance spectrum of Bi nanowire arrays in AAO templates measured by FTIR spectroscopy. (i) Al mirror reference spectrum, (ii) reflectance from AAO template with backside metal on top: negligible effect of bottom electrode and substrate on IR absorption, (iii) periodicity in reflectance: interference in reflected signal (AAO film effect), (iv) AAO only: larger reflectance compared with Bi samples, (v) Bi nanowires in AAO (diameter: 50 nm), (vi) Bi nanowires in AAO (diameter: 38 nm), (vii) Bi nanowires in AAO (diameter: 67 nm), and (viii) IR spectra over 500 ~ 1800 cm^{-1}: significant absorption by AAO.

Photo-absorption spectral dependence on the diameter has been measured. The preliminary spectral data appears to be consistent with theoretical expectations in general. For example, a transition from metallic to narrow bandgap (E_g ~ 0.3 eV, or E_g ~ 4.1 eV) semiconducting is revealed in the Tauc plot of the measured spectra, as shown in figure 8.

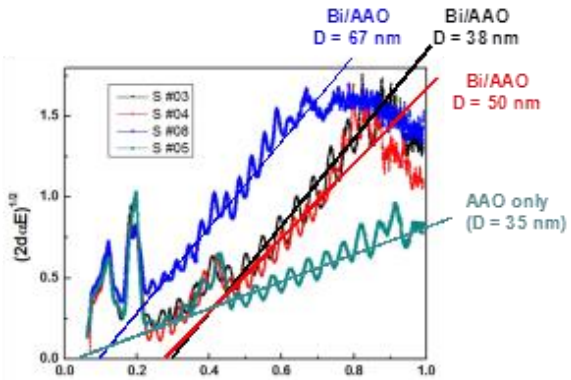

Figure 8 Tauc plot of absorption of arrays of nanowires in AAO templates, indicating band gap.

3.5 Contact properties:

Geometry and size effects:

For over a decade, semiconducting nanowires NWs have been widely pursued as promising candidates for a variety of device applications such as NW-based transistors, photodetectors, and biosensors. In addition to improving NWs' intrinsic physical properties, it is also a very important issue to minimize or optimize metal-NW contact effects since the sensitivity of sensors and the performance of transistors are strongly dependent on the series contact resistances. Usually, the high contact resistance of NW devices has been attributed to the small contact area, because contact resistance is inversely proportional to contact area and the contact width of a NW device is limited by the circumference of the NW. However, progress in physical understanding and modeling of electrical properties of metal contacts on NWs lags behind the demonstration of prototypes and new potential applications of NW-based devices.

To this end, we studied [4] the electrical properties of metal contacts on doped NWs that are not fully depleted by the contact formation. Our findings indicate that 1) a NW is fully depleted at lower built-in potential and higher dopant concentration than a planar SC, leading to a drastic increase in contact resistance, which hinders the use of the conventional TLM for analysis of the contact properties, 2) the differences in the width of the depletion regions and the IFBL effects play a dominant role in the larger contact resistance in the NW device at room temperature, and 3) the geometrical dependence of

contact resistance is more significant at low temperatures due to the reduced thermionic and TFE effects. The theoretical study of

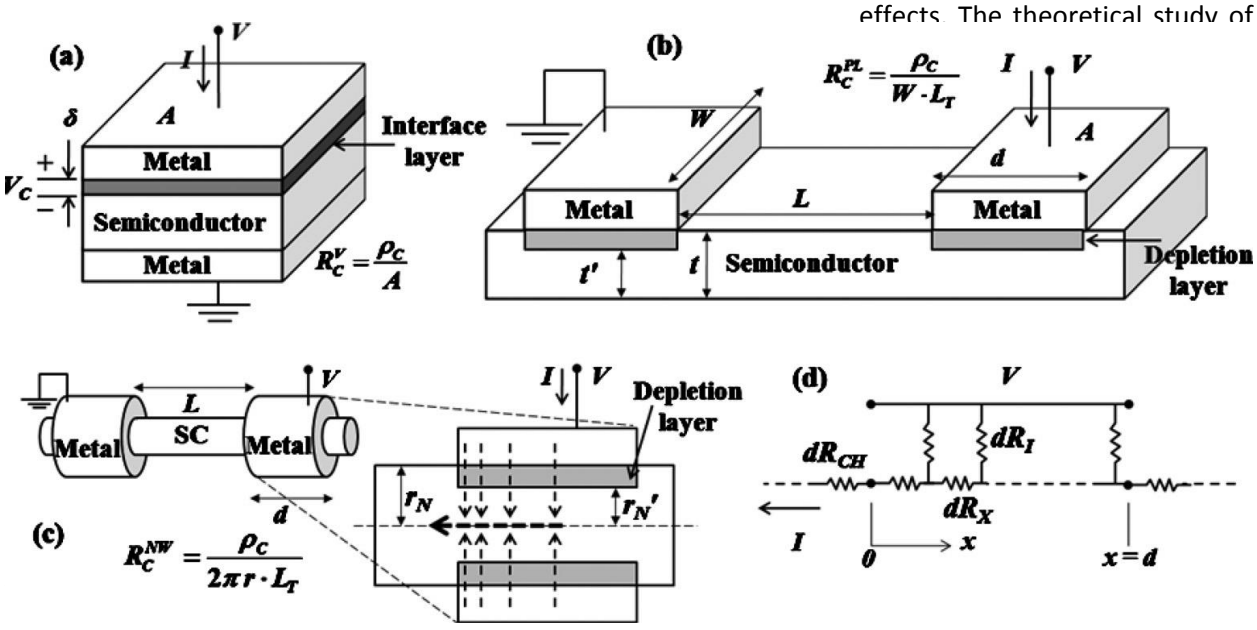

Figure 9 Schematic diagrams of (a) vertical planar metal-SC, (b) lateral planar metal-SC, and (c) lateral cylindrical metal-NW structures. (d) The equivalent lumped circuit of the metal-SC contact regions.

the small dimensions of the neutral semiconducting region of the NWs—which is comparable to the

width of the depletion region—and to the use of the same doping concentration in the channel and contact regions. The study also suggests that the formation of a higher doping concentration in the contact regions is essential for better Ohmic contacts on NWs. Our work shows why one should revisit the effects of geometry and size of the SCs on the electrical contacts and their influence on the overall transport behavior of low-dimensional SC devices.

Contact effect measurement methods:

It is known, but often unappreciated, that the performance of nanowire (NW)-based electrical devices can be significantly affected by electrical contacts between electrodes and NWs, sometimes to the extent that it is really the contacts that determine the performance. To correctly understand and design NW device operation, it is thus important to carefully measure the contact resistance and evaluate the contact parameters, specific contact resistance and transfer length. A four-terminal pattern or a transmission line model (TLM) pattern has been widely used to measure contact resistance of NW

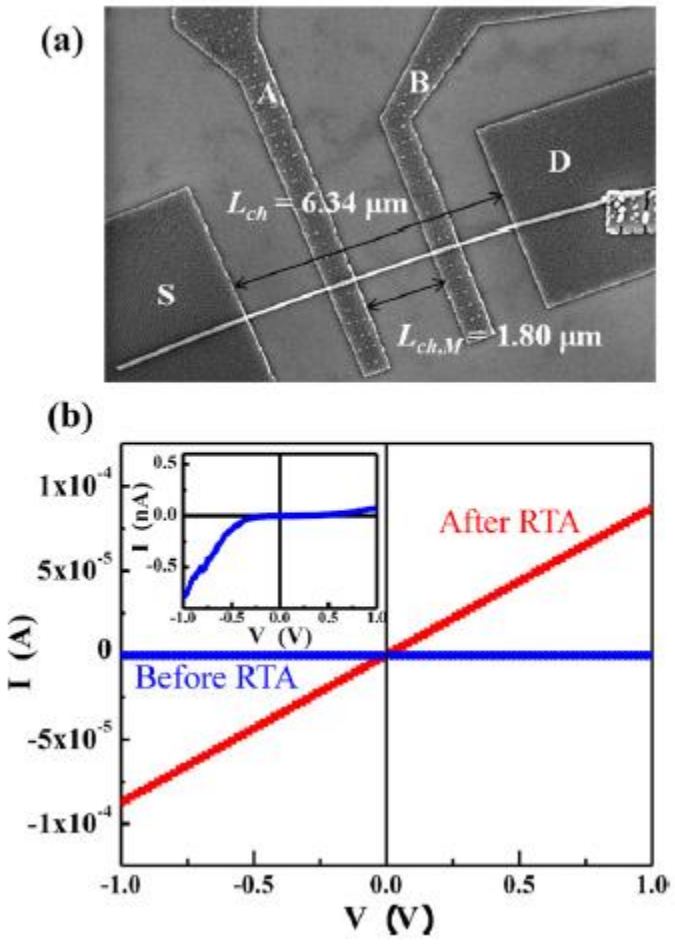

Figure 10 (a) Scanning electron microscopy image of a four-terminal pattern on a GaN NW deposited on an oxidized Si substrate. (b) I–V characteristics of the GaN NW two-terminal device after rapid thermal annealing. (Inset: the magnified I–V plot of the device before annealing.)

ices and the TLM has been typically used extract contact parameters of NW devices. wever, the conventional method assumes electrical properties of semiconducting ions covered by a metal are not changed ctrode formation. In this study, we report conventional methods for contact luation can give rise to considerable errors ause of an altered property of the NW electrodes. We demonstrate that more rect contact resistance can be measured n the TLM pattern rather than the four- minal pattern and correct contact ameters including the effects of changed properties under electrodes can be luated by using the contact end resistance asurement method.

We have discussed [1] the issues in conventional method to measure contact stance and analyze contact parameters of ctrical contacts on semiconducting NWs. It hown that the four-terminal method can se considerable error in the measured ntact resistance because the electrical operties of the NW under the inner electrodes are included in the calculation of the NW channel resistance. It is also shown that the contact parameters can be more correctly evaluated from the contact end resistance measurement than from conventional bulk TLM since the parameters can be extracted from the electrical properties of the NW in the contact regions. The suggested procedure of contact evaluation will improve the accuracy of the measured contact resistance

and analyzed contact parameters of electrical contacts on nanoscale semiconductors such as nanowires, nanotubes and thin films.

4. Bi_2S_3 nanowires:

4.1 Introduction:

Metal sulfides have great potential for various applications. Numerous sulfur source molecules have been employed for metal sulfide synthesis, but there are still some problems, including hazardous byproducts and harsh experimental conditions. Discovering an environmentally friendly new sulfur source molecule is critical for metal sulfide synthesis.

Bismuth sulfide is a semiconducting material, has a direct band gap of 1.3 eV [10] and has been used in photodiode arrays or photovoltaic devices [11, 12]. It also belongs to a family of solid-state materials with applications in thermoelectric technologies based on the Peltier (cooling) effect [13] since bismuth-based materials exhibit good thermoelectric power. Like other materials, bismuth sulfides have been fabricated into 1D nanostructures in recent years. There have been several reports on the synthesis of one-dimensional nanostructured Bi2S3, including single-source precursor approach [12], hydrothermal/solvothermal process [14, 15], and chemical vapor deposition method [16].

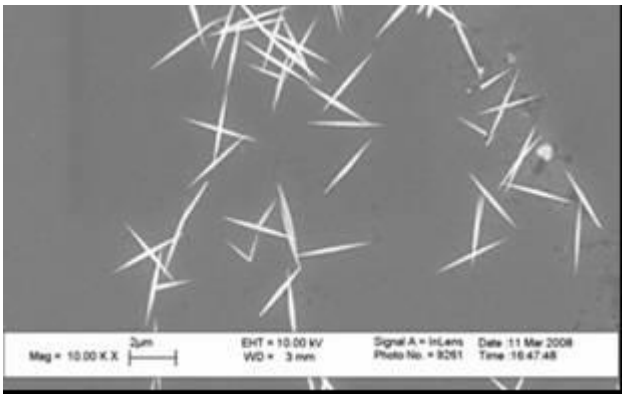

Figure 11 SEM image of typical Bi_2S_3 nanowires deposited on

Differing from these prior works, we have successfully synthesized single-crystalline Bi2S3 nanostructures with high uniformity of diameter and high-aspect ratio using a new sulfur source molecule, 2-mercaptoethanol, in a low-temperature, solvothermal reaction process without a template. We found that the morphology of bismuth sulfide can also be successfully tuned into tapered, cross and T-shaped nanowires (as well as other interesting structures) with the use of a biomolecule, glutathione (GSH), instead of varying temperature and concentration that are more traditional but difficult to control precisely. An atomic structural study of the crystallinity confirmed that the BiS nanowires fabricated this way is single crystalline. Its electrical properties were investigated in detail, by fabricating and comprehensive tests of field-effect-transistors and photodetectors.

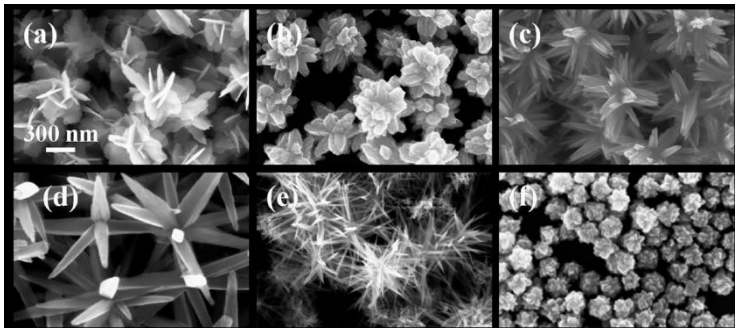

Figure 12 Bi2S3 nanostructures produced from the solution containing (a) GSH-O only (Bi/GSH-O) 1:3), (b) Bi/GSH-O/ME) 1:3:2, (c) Bi/GSH-O/ME) 1:3:20, (d) Bi/GSH-O/ME) 1:3:72, (e) Bi/GSHO/ME) 1:3:120, and (f) GSH-R only (Bi/GSH-R) 1:6). Synthesis conditions: 130 °C, 7 h. The scale is the same in all panels.

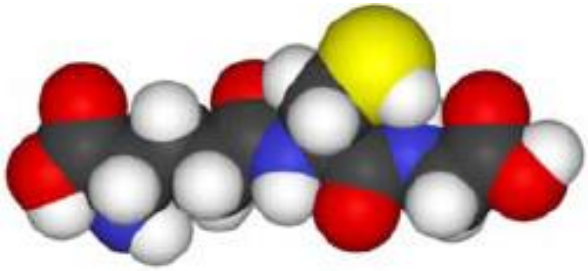

Figure 13 Glutathione molecule.

The additional advances came somewhat unexpectedly in an experimental exploration of a new synthesis pathway for bismuth-based nanostructures. They opened up a new space in which bismuth sulfide (Bi2S3) nanostructures of high uniformity and crystallinity can be made available for a variety of device applications and basic research.

4.2 Synthesis:

This synthesis technique is template-free and the control of size and morphology is thermochemical. These nanostructures were prepared by biomolecule-assisted synthesis, which resulted in surprisingly high crystallinity and good uniformity, with diameters of (50 ± 10) nm and lengths of (1.9 ± 0.2) µm. To assess their electrical properties, we fabricated nanowire transistors with a back-gate structure. The as-grown nanowires are found to be n-type semiconductors and the on-off ratio of the transistors is about 10^2 with a silicon dioxide layer of 50 nm thickness as the gate insulator. More complex and functional nanowire structures are also being developed by this biomolecule-assisted synthesis, including a three-terminal nanowire structure.

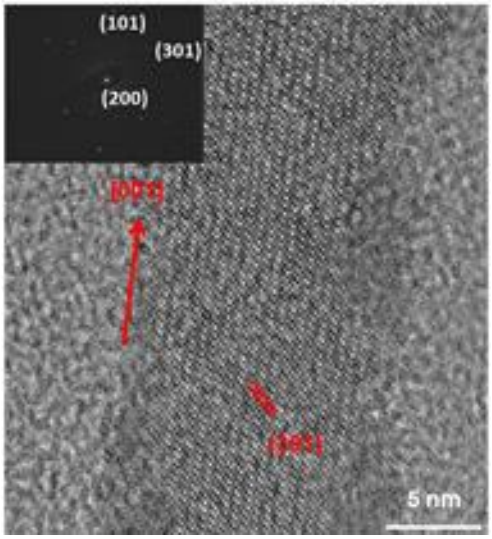

Figure 14 High resolution TEM image and the corresponding SAED pattern (inset).

Bi_2S_3 has been prepared in glycerol-based aqueous solutions at temperatures between 110 ºC and 150 ºC. 2-Mercaptoethanl, glutathione-reduced (GSH-R), and glutathione-oxidized (GSH-O) were employed as sulfur source. Surfactants, poly(vinylpyrrolidone) (PVP), oleic acid and oleyl amine were tried to tune morphology of Bi_2S_3. In typical experiment, appropriate amount of $Bi(NO_3)_3$ and sulfur source molecules of

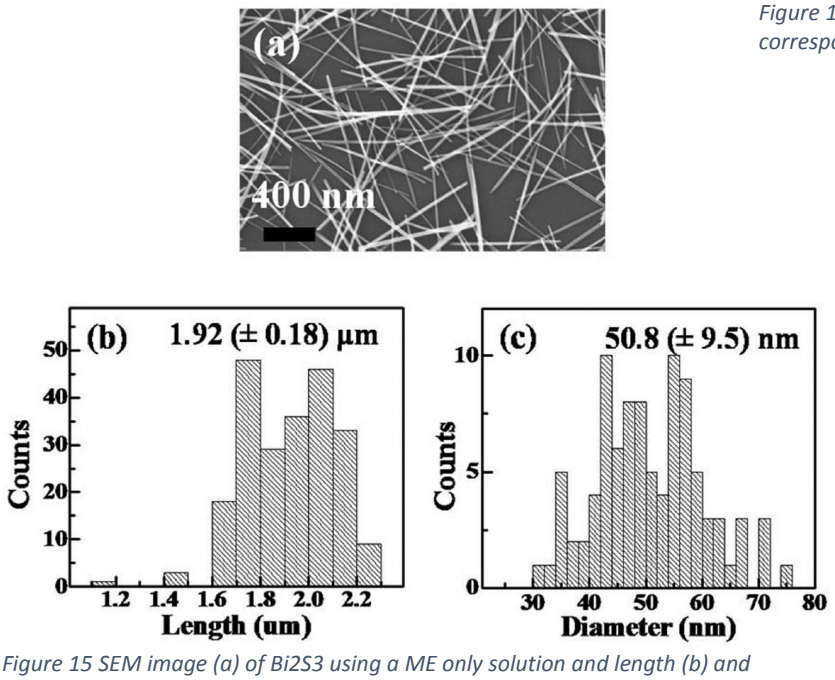

Figure 15 SEM image (a) of Bi2S3 using a ME only solution and length (b) and diameter (c) distributions. Synthesis conditions: 130 °C, Bi/S) 1:72, 7 h.

micromolar range were mixed with 15 mL glycerol in glass bottle and the glass bottle was soaked into oil bath of designated temperature (molar ratio of Bi source:2-mercaptoethanol source = 1:70, 140 ºC). The SEM image of the synthesized nanowires and the histogram of the nanowire length and diameter are shown in figure 15 which reveals good uniformity, with diameters of (50 ± 10) nm and lengths of (1.9 ± 0.2) µm.

Kinetics of nanowire growth was investigated by examining SEM with growth time and it is shown in figure 16. For a given synthesizing condition, the growth rate is constant in early phase (<100 min) then the growth saturates. Constant growth rate enables control of the diameter and length by growth time and the saturation of growth makes it possible to obtain uniform dimensions of the synthesized nanowires.

The crystallinity of the grown nanowires was confirmed by HRTEM image of a single Bi_2S_3 nanowire, which has lattice plane with spacing of 0.27 nm, corresponding to the d spacing of the (301) of orthorhombic phase, as seen in Figure 14. The inset in the figure 14 shows corresponding SAED pattern taken along the [010] zone axis. The Bi_2S_3 nanowire was preferentially grown along the [001] crystal axis.

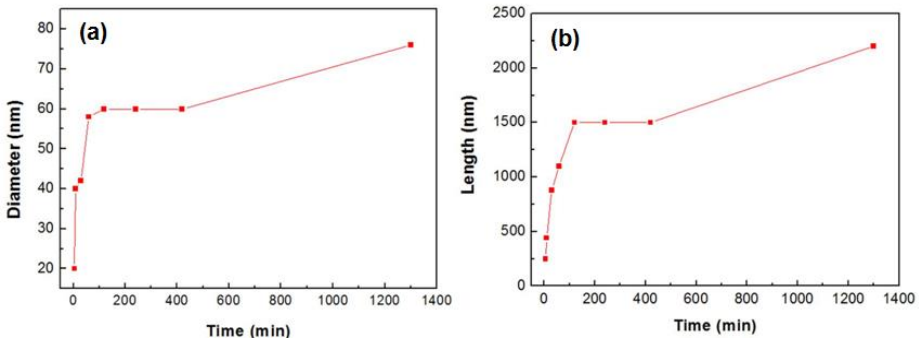

Figure 16 (a) SEM image of the synthesized Bi2S3 nanowires and (b) histogram of nanowire diameter (b) and length (c)

4.3 Optical characteristics:

Despite the many years of effort and studies that have been reported in a large body of literature, the underlying mechanism of large photoconductive gains observed in nanowire photodetectors has not been clearly explained yet. It is generally thought to be the result of a long carrier lifetime due to deep traps as in often is the case in bulk semiconductors. In this work, we demonstrated that the photoconductive gain of a Bi_2S_3 NW photodetector can be significantly enhanced by optical modulation of electrical injection through contacts. We proposed a quantitative model to explain the results based on a detailed analysis of metal-nanowire contacts. The study shows optically generated excess carriers can modify the contract barrier energy profile at the metal-nanowire interface and thereby increase photoconductivity.

This finding is applicable to all nanowires and their photoresponses. As nanowires generally exhibit high photosensitivity and large intrinsic polarization anisotropy [31, 32] all kinds of semiconducting NWs such as Ge [33], InP [32], ZnO [13], CdS [14], GaN [15], and Bi_2S_3 [16, 17], are in development for photoconductive-type sensing applications. As such, this generally applicable finding of an intrinsic functionality of nanowires could be especially meaningful and timely.

Typically, the diameters of NWs (10 ~ 100nm) are much smaller than the inverse of the absorption coefficient of the materials (~ um). Therefore, their large photoconductive gain has been explained by a long carrier lifetime resulting from high density of deep trapping centers [13, 18, 33]. The commonly suggested mechanism is that one type of optically generated carriers is captured by surface or bulk trap states and the opposite carrier has long carrier lifetime but shorter transit time. The excess carriers traverse through the wire and their resupply from the electrode to minimize charge imbalance thereby gives rise to a large photoconductive gain. An alternatively or additionally suggested qualitative explanation on enhanced photoconductivity of NWs [15] and bulk semiconductors [19, 20] could be modulation of electrical contacts by optical input. It is now widely accepted that electrical contacts play a significant role in NW electronic operations. In dark, it has been shown that NW devices have greater contact effects compared to planar devices due to the small dimensions and the cylindrical geometry [4, 21, 22]. To our best knowledge, however, there has been no report on a quantitative model and study for electrical contact effects on a NW photodetector yet. In this work, we showed that optical modulation of electrical injection over contacts can be a major contributor to the optical gain of a semiconducting NW. Furthermore, we introduced a model of optical modulation of the metal-NW contact to explain the observed results.

We used bismuth sulfide (Bi_2S_3) NWs as a model material for this study. The NWs were chemically synthesized in a solvothermal process with an excellent uniformity of the diameter along the entire NW length. The NWs' band gap extracted from UV-visible absorption spectrum was about 1.55 eV. The experimental details and material characterizations of the synthesized NWs were published in [3]. For device fabrication, the NWs were dispersed on an oxidized Si substrate (thickness of the SiO_2 = 50 nm) and electrodes (Pd) were then patterned on an individual NW by using electron beam lithography and a lift-off process (the inset of figure 17(a)). From I-V characteristics of the back-gated field effect transistors (FET), the polarity (n-type) and carrier concentration (~3.5×10^{18} cm^{-3}) of the synthesized NWs were estimated.

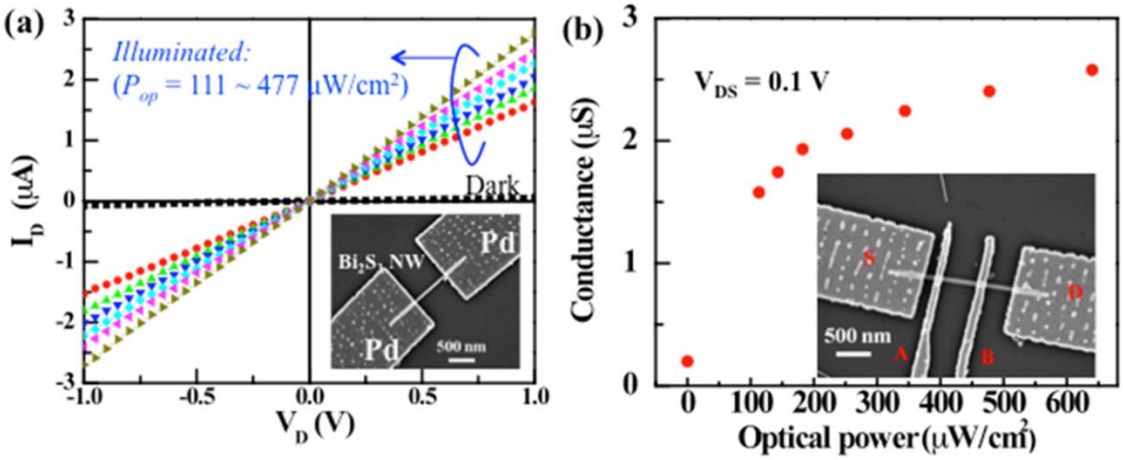

Figure 17 (a) Current-voltage characteristics of a B_2S_3 NW photodetector under dark and illuminated conditions. (Inset: SEM image of a fabricated NW photodetector. The diameter is about 50 nm.) (b) Conductance between electrodes S and D as a function of optical input power at bias voltage of 0.1 V (Inset: SEM image of the four-terminal device. The diameter is 52 nm.)

The I-V characteristics of the fabricated device were measured in dark condition and under illumination of visible light that has broad wavelength range of 400 - 800 nm and peak intensity at 600 nm. The dark *I-V* showed an Ohmic conduction and the current was significantly increased under illumination (Figure 17(a)). To evaluate the effects of electrical contacts on the photoconductivity, we fabricated a four-terminal pattern on a Bi_2S_3 NW (diameter ~52 nm) (figure 17(b)). The device

conductance as a function of the optical power and the *I-V* curves showed behavior very similar to that of the two-terminal device. The saturation of the conductance at a higher illumination intensity may indicate that the optical response mechanism is associated to a carrier trapping, since the density of trapped holes is limited by the trap density [18]. Under dark and illuminated conditions, the channel resistivity was calculated from the voltage drop between two middle electrodes and constant current input applied to the electrode *D*. Since the input impedance of the voltage measurement units of the semiconductor parameter analyzer (Agilent 4156C) we used is larger than 1 GΩ, the monitored current through the middle electrodes was smaller than 1% of the input currents. Therefore, the contact resistances of the middle electrodes can be ignored. Figure 19(a) shows the change of the channel resistance and contact resistance with the optical power. The resistances were measured at V_{DS} = 0.1 V and very similar results were obtained at a larger bias (1 V). What is revealing was that the contact resistance decreased more sharply than the channel resistance under illumination. The fraction of the total device resistance contributed by the contact resistance in dark and under illuminated is shown in figure 19(b). About 85% of the device resistance resulted from the contact resistance in dark and the fraction by the contact resistance decreased to about 50% under illumination. This means that more than 90% of the photoconductivity change came from the contact resistance change. Figure 19(c) shows the dependence of the channel resistivity and carrier concentration on the optical power. The results clearly show that a significant fraction of the photoconductance change comes from the change of contact resistance even though the channel resistance is also decreased by the optical input, the latter of which can be accounted for by the more conventional model of a long carrier lifetime in deep traps.

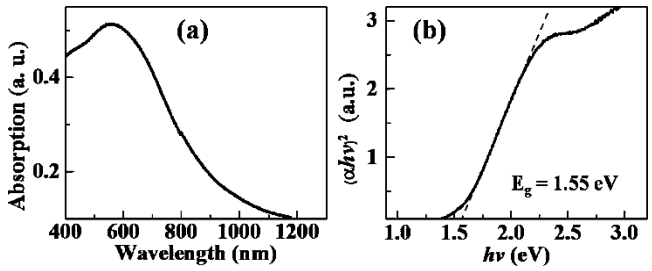

Figure 18 (a) Absorption spectrum of bismuth sulfide nanowire solution. (b) Plot of (Rhv)² versus hv.

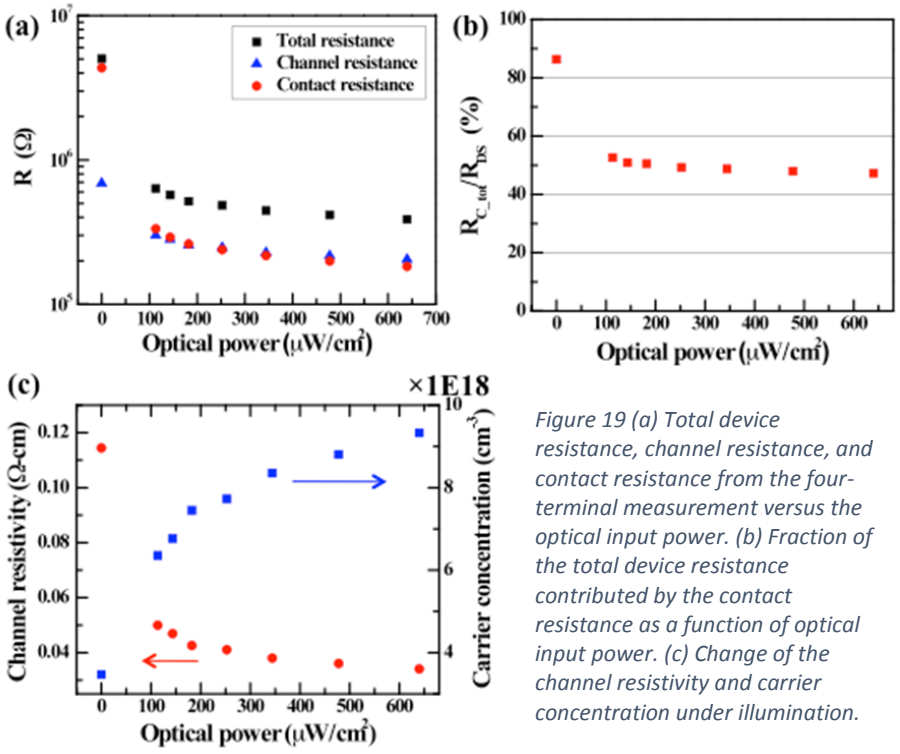

Figure 19 (a) Total device resistance, channel resistance, and contact resistance from the four-terminal measurement versus the optical input power. (b) Fraction of the total device resistance contributed by the contact resistance as a function of optical input power. (c) Change of the channel resistivity and carrier concentration under illumination.

To summarize, we have demonstrated that the photoconductive gain of a NW photodetector can be due to optical modulation of carrier injection through the contact. We explained the contact effects based on a NW-metal contact model. The result shows that optically generated carriers modify the barrier structures (built-in potential and depletion width) and thereby enhance the thermionic

emission and decrease the spreading contact resistance in the contact regions. The work points to the importance to take into account the effects of optical modulation of electrical contacts in evaluating the performance of a semiconducting NW photodetector.

In addition, optical absorption experiments were carried out to elucidate information on the band gap energy, which is one of the most important electronic parameters for semiconductor nanowires. Figure 18 (a) shows the spectrum of bismuth sulfide nanowire solution (in methanol). For a direct bandgap semiconductor, the bandgap energy is usually defined by the x-axis intercept of $(\alpha h\nu)^2$ versus $h\nu$, where α is absorption coefficient. [17, 18]. From figure 18 (b), we estimate the band gap is 1.55 eV.

4.4 T junctions and novel nanostructures:

We accidently discovered that it is possible to make a three-port nanowire by synthesis, as exemplified here in a zoomed-in SEM image. With such a T-junction nanowire structure, direct electrical connection can now be made to each of the three ports. Having a third port directly built-in, one can now easily envision real-time spectral tuning via the electro-optics (e.g. dielectric polarization) effect and/or the plasmonic (collective electron motions) effect that are modulated by the voltage or current applied to the third terminal. In the latter case, we further envision that the T-junction material could be replaced with ones that are more favorable for plasmonic excitation. This could be achieved, for example, by using the synthesized T-junction as a scaffold for evaporation of silver or other metals.

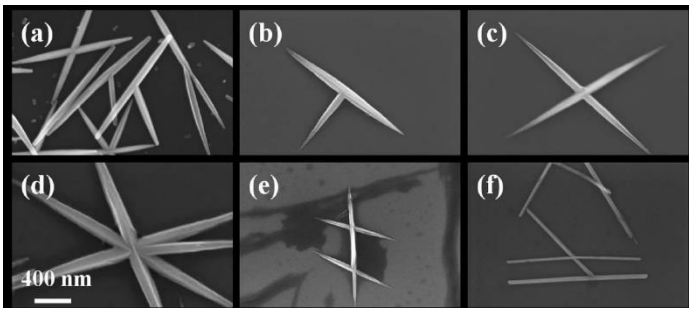

Figure 20 Branched nanowires from a solution of Bi/GSH-R/ME) 1:6:72. Synthesis conditions: 130 °C, 7 h. The scale is the same in all panels.

Figure 21 shows the morphology evolution with sulfur source molecules. Surprisingly, we found that the addition of small amounts of GSH-O or GSH-R to the solution containing only ME caused a tapered nanowire-urchin structure to form. This result is very interesting in that it demonstrates the ability of small biomolecules to serve as effective morphology-tuning agents of nanostructures in general solvothermal or hydrothermal syntheses. This is to be contrasted with other approaches utilizing much larger surfactant molecules. At a lower ratio of GSH-O to ME, a blunt nanowedge-urchin structure (Figure 21(b)) evolved from the nanoleaf-urchin grown in GSH-O solution (Figure 21(a)). By increasing the ratio of ME to GSH-O, the morphology changes from a short nanowedge-urchin to a long nanowire-urchin structure (Figure 21(b)-(e)), and ultimately, a ME only solution gives long nanowires (Figure 20(a)). The addition of GSH-R to the ME-only solution showed similar effects on the morphology, and this is because GSH-O is converted into GSH-R in the presence of ME, which is known to be an efficient disulfide-breaking agent. Previously, urchin-like structures have been prepared by a rapid polyol process. This is rather different from previously reported Bi_2S_3 structures using GSH-R in which the authors used a microwave digestion system at 120 °C in a water-based solution and made snowflakes, spindles, nanorods, and nanowires, dependent upon the ratio of Bi/GSH-R, but they did not report an observation of nanoleaf-urchin or nanoparticle structures. This difference may have resulted from different heating methods and solvent compositions.

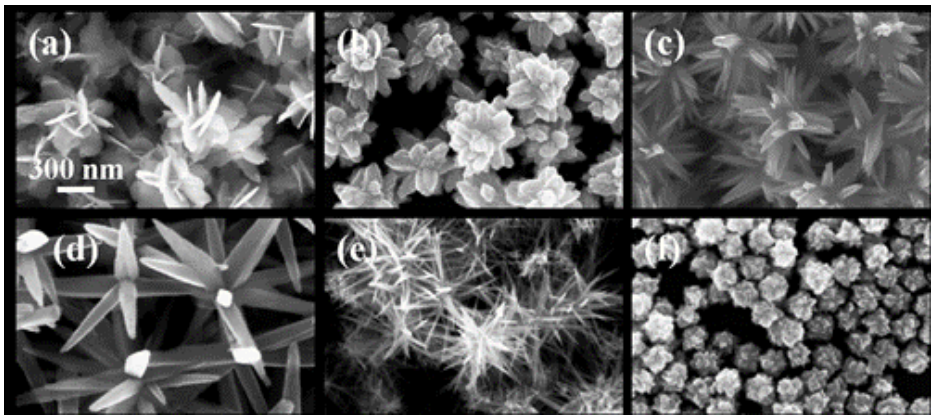

Figure 21 Bi_2S_3 nanostructures produced from the solution containing (a) GSH-O only (Bi/GSH-O) 1:3), (b) Bi/GSH-O/ME) 1:3:2, (c) Bi/GSH-O/ME) 1:3:20, (d) Bi/GSH-O/ME) 1:3:72, (e) Bi/GSHO/ME) 1:3:120, and (f) GSH-R only (Bi/GSH-R) 1:6). Synthesis conditions: 130 ℃, 7 h. The scale is the same in all panels.

5. Bi on AAO superconducting-insulating transition:

5.1 Superconducting-insulating transition:

In what was cited as one of the 'top-ten physics stories of [the year]' by the American Institute of Physics, our group, in collaboration with another group at Brown University, reported on a novel superconductor to insulator transition taking place in thin Bi films deposited on AAO [11]. We found that nano-scale periodic patterning of bismuth could induce a dramatic transition from

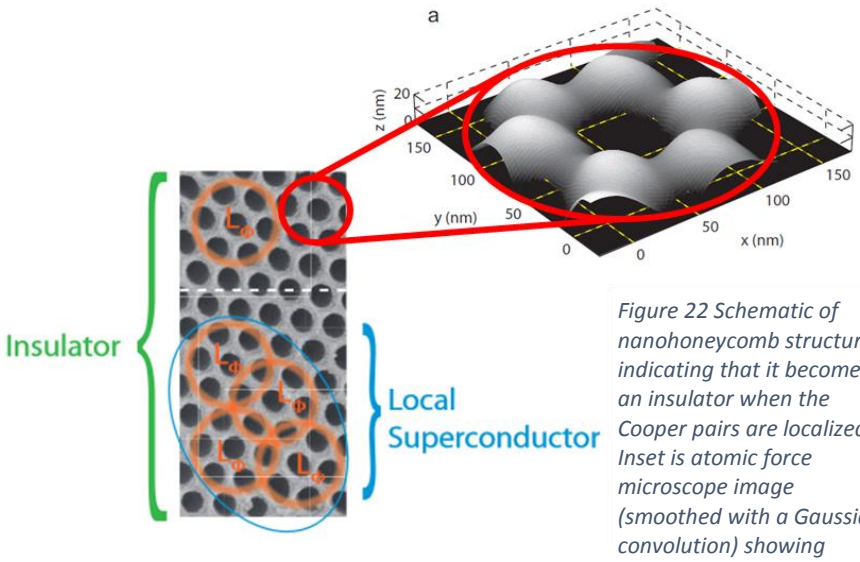

Figure 22 Schematic of nanohoneycomb structure, indicating that it becomes an insulator when the Cooper pairs are localized. Inset is atomic force microscope image (smoothed with a Gaussian convolution) showing regular surface undulations around each hole.

superconducting to insulating due to localization of the Cooper pairs. The nano-patterning was done by evaporating thin films of Bi on AAO, which caused there to be dips in the film above the positions of the AAO pores, a so-called “nano-honeycomb pattern”. These valleys caused localization of the Cooper pairs which are the fundamental carrier of superconducting currents – thus, their localization causes the film to act as it would without the superconducting aspect, which is a strong insulator, due to its thinness.

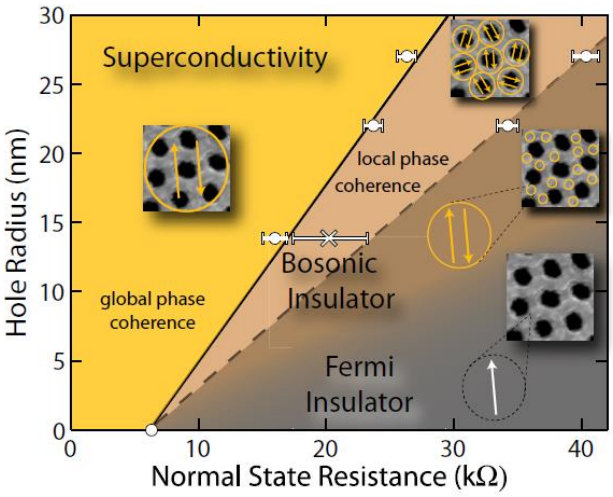

Figure 23 Phase diagram for NHC and conventional Insulator-Superconductor transitions.

5.2 THz sensing and generation:

The effect of interrupting the delicate superconducting current is frequently used for THz single photo detection, and could be used here as well. In uses for single photon detection, a photon striking the superconducting region temporarily locally heats the region up, causing the region to not be superconducting. This causes most of the bias current to be routed elsewhere, the difference of which is easily measurable. In fact, this is the fastest method of single-photon detection to date and has been shown to be very effective in the near-IR (100’s of THz!) [34].

Our work published in [10] is easily extended to this. In this study, we have performed a systematic study of the suppression of the critical temperature of weakly superconducting, amorphous thin films through regular mesoscopic thickness fluctuations. With this background, the detection edge at which the incident photon has sufficient energy to break the superconducting current could be tuned by altering parameters such as the AAO pore width, spacing, or the Bi film thickness. This concept could be realized in a system with a multiplexed system of differently tuned superconducting single photon detectors.

Indeed, superconducting layers have been used to detect THz radiation using another mechanism as well [35]. In this mechanism, superconductive layers are separated by insulating layers, which superconducting current can tunnel through. However, this inter-layer tunneling can be weakened by a strong electric field, which can cause the interlayer tunneling to be interrupted. This mechanism was activated using 2 THz pulses in this paper. This system could be realized in confined ultra-thin Bi films on AAO, using the foundation laid by our work.

Likewise, this effect has been harnessed to emit THz radiation as well [36]. The Josephson effect is well known, in which an applied DC voltage can give rise to an AC voltage and thus tunable electromagnetic radiation. The same layered structures have proven to potentially be compact sources of coherent continuous-wave electromagnetic radiation in the subterahertz and terahertz frequency ranges. Thus, stacked Bi NHC films could be used as a platform for this mechanism.

6. Giant magnetoresistance in Bi on AAO:

Magnetoresistance measurements of quantum confinement effects:

Bi's interesting magnetic properties have long been known. It is the most naturally diamagnetic element, and has been known to display negative magnetoresistance in quench-condensed films in the immediate vicinity of the thickness-tuned superconductor-insulator transition [37].

A former member of our laboratory discovered [7] that thin Bi films deposited on AAO created what was called an "anti-dot" structure, referring to the fact that the films on top of the AAO had the pattern of the inverse of a 2D lattice of dots. This is inherently an interesting structure, because though it is already confined in the out-of-plane due to the thinness of the deposited film, the film is also punctuated by an array of holes which confines it further. In this study it was observed that the anti-dot thin film with the AAO pore wall widths and film thickness smaller than the Fermi wavelength of Bi showed low dimensional electronic behavior at low temperatures.

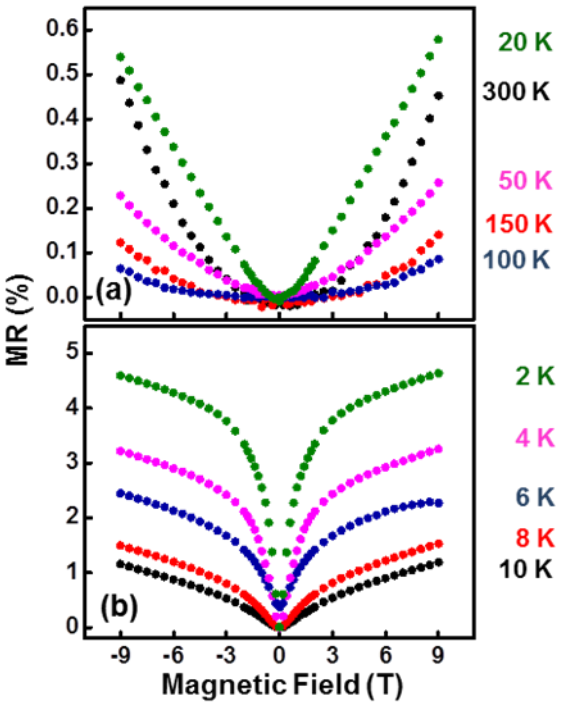

Figure 24 Magnetoresistance vs field curves of 38 nm pore wall width/25 nm thickness Bi anti-dot film at various temperatures; (a) from 300K to 20K, (b) from 10K to 2 K.

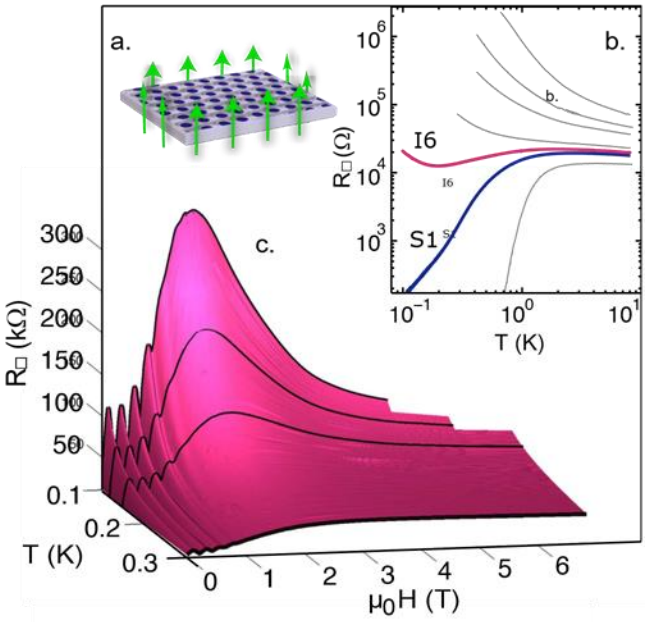

Figure 25 a) SEM image of the nano-honeycomb substrate. The hole center to center spacing and radii are 100 ± 5 and 27 ± 3 nm, respectively. Arrows denote H~ . b) Sheet resistance as a function of temperature, R(T), of NHC films produced through a series of Bi evaporations. The film I6 is the last insulating film and S1 is the first superconducting film in the series. c) Surface plot of for film I6, which has a normal state sheet resistance of 19.6 kΩ and 1.1 nm Bi thickness. The solid lines are isotherms.

Giant Magnetoresistance in a Cooper Pair Insulator:

Ultrathin amorphous Bi films, patterned with a nano-honeycomb array of holes, can exhibit an insulating phase with transport dominated by the incoherent motion of Cooper Pairs (CP) of electrons between localized states. In this study [38], we showed that the magnetoresistance (MR) of this Cooper Pair Insulator (CPI) phase is positive and grows exponentially with decreasing temperature, T, for T well below the pair formation temperature. It peaks at a field estimated to be sufficient to

break the pairs and then decreases monotonically into a regime in which the film resistance assumes the T dependence appropriate for weakly localized single electron transport. We discuss how these results support proposals that the large MR peaks in other unpatterned, ultrathin film systems disclose a CPI phase and provide new insight into the CP localization.

In summary, we have shown that the magnetoresistance of amorphous nano-honeycomb Bi films exhibits a giant, positive peak, which is similar to that observed in other unpatterned, ultrathin film systems near the superconductor to insulator transition. The main result is the verification that this peak arises from the low field positive magnetoresistance of a Cooper Pair Insulator phase with transport dominated by incoherent tunneling of Cooper pairs and a high field negative magnetoresistance associated with the destruction of the pairs. While these conclusions agree qualitatively with some models, fundamental questions about the processes driving the Cooper pair localization, the emergence of the Cooper Pair Insulator phase at high disorder and the size of the localized states require further experimental and theoretical attention.

7. Percolation and dielectric anomaly in Bi UTMF:

It was reported [12] that gold and lead films of thickness in the 10's of Angstroms range were exhibiting interference effects in the THz range. This was attributed to what has been called a "dielectric anomaly", in which the real part of the dielectric constant of the material diverges, causing the refractive index and thus the optical path length to diverge, allowing light of extraordinarily large wavelengths (compared to the film thickness) to interfere with it. This phenomenon generally occurs when a material undergoes a critical phase change between an insulating and conducting pause. In this case, it was proposed that the phase transition was between the tunneling (unconnected) and percolation phases of the film, due to it being so thin that it was not a continuous film yet but composed of deposited "islands" forming clusters of varying connectivity.

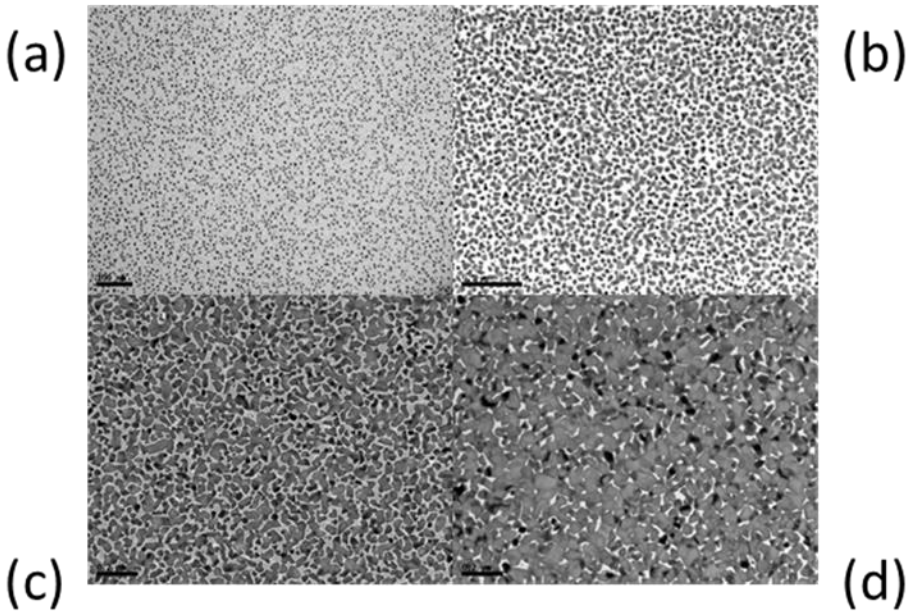

Figure 26 TEM images after different deposition times. Nominal deposited thicknesses are (a) 10Å, (b) 40Å, (c) 80Å, (d) 130Å.

One intuitive interpretation of this phenomenon has been that, as more material is deposited and the clusters that form the growing film get closer together, the capacitance between adjacent unconnected clusters increases as 1/d, which in turn causes the reactance to

decrease, which causes the imaginary part of the conductivity to increase, which causes the real part of the dielectric contestant to increase.

Our group recently investigated percolation in evaporated Bi films, with the intention of using this base as a springboard to expand this research to investigate the dielectric anomaly, now that we have characterized the percolation transition. Though a similar system has been studied before, in the form of evaporated Bi nanoparticles sandwiched between two insulating and transparent Al2O3 layers (to prevent total oxidation which would occur instantly for such small particles) [39], they did not investigate the optical properties exactly at the threshold, which would be necessary to observe this phenomenon, as the divergence is narrow and steep.

8. THz generation from thin Bi films:

It is known that there are several methods that can give rise to THz generation in nanopatterned thin Bi films: excitation with a short pulse laser[40, 41], hydrodynamic nonlinearity of a 2D electron fluid [42], and excitation of surface plasma waves by a parallel propagating electron beam [43]. To this end, in a collaborative effort with researchers at other schools, our group used combinations of methods including e-beam lithography (EBL), focused ion beam (FIB) milling, and reactive ion etching (RIE) to create highly customizable structures such as Bi quantum dot lattices, butterfly antennae, and anti-dot lattices, as shown in figure 26. These techniques of exciting THz radiation are currently being investigated using these fabricated Bi nanostructures.

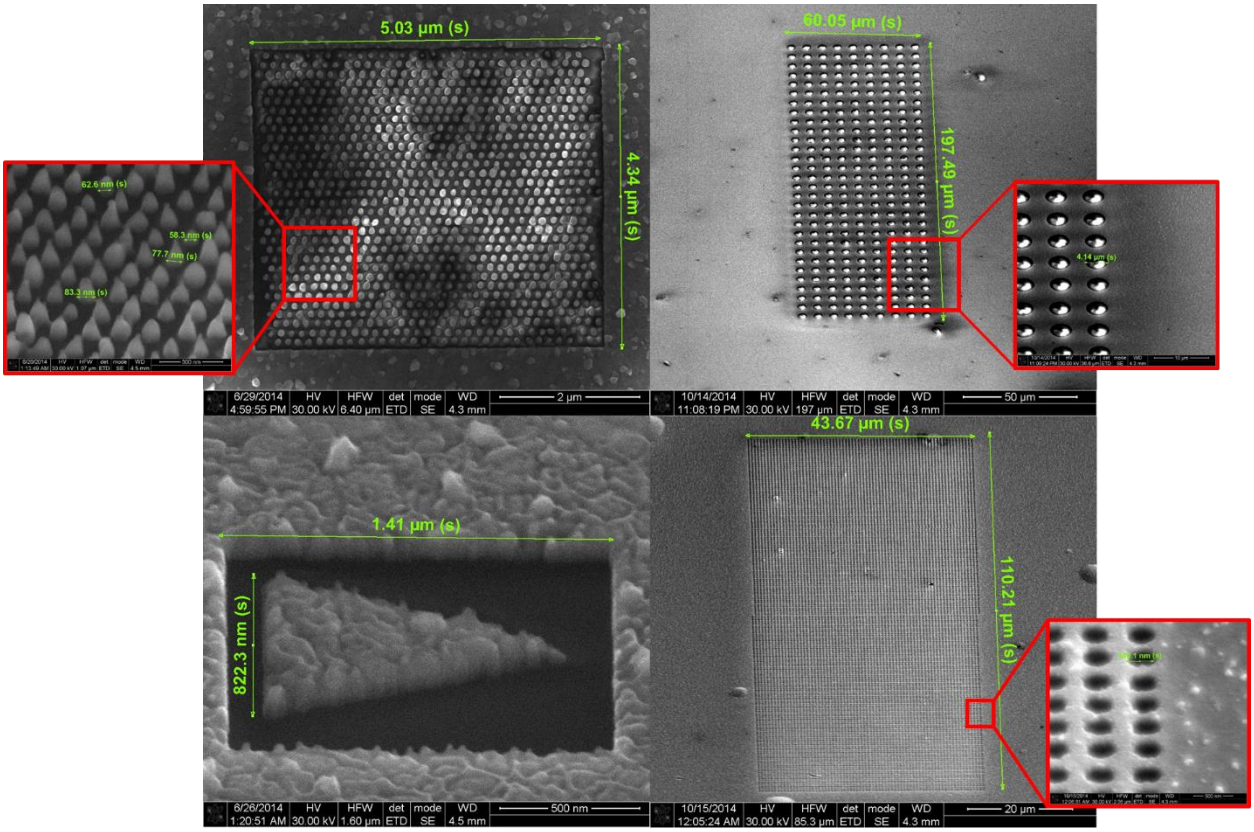

Figure 26 SEM images. (top left): Bi dot structure, inset shows feature sizes magnified. (top right), (bottom right): Bi anti-dot structure, for plasmonic excitation and coupling. (bottom left): nano-antenna.

9. Publications, papers, and talks arising from this project:

Publications in Refereed Journals and Refereed Series:

1. Jin H. Kim, Hongsik Park, Chih-Hsun Hsu, and Jimmy Xu, "Facile Synthesis of Bismuth Sulfide Nanostructures and Morphology Tuning by Biomolecule", *J. Phys. Chem. C*, 2010, *114* (21), pp 9634–9639
2. Hongsik Park, Roderic Beresford, Seungbum Hong, and Jimmy Xu,"Geometry-and-size-dependence of electrical properties of metal contacts on semiconducting nanowires" J. Appl. Phys. 108, 094308, 2010.
3. Sovan Kumar Panda, Dongil Han, Hyunjun Yoo, Hyunjung Shin, Hongsik Park, and Jimmy Xu, "Synthesis of Step-Shaped Bismuth Nanowires—An Approach Towards the Fabrication of Self-Homojunction", Electrochemical and Solid-State Letters, 14 (6) E21-E24 (2011)
4. S. M. Hollen, H. Q. Nguyen, E. Rudisaile, M.D. Stewart, J. Shainline, J.M. Xu, J.Valles, "Cooper-pair insulator phase in superconducting amorphous Bi films induced by nanometer scale thickness variations", Phys. Rev. B 84, 064528 (2011)
5. H.S. Park, J.H. Kim, R. Beresford, J.M. Xu, "Effects of electrical contacts on photoconductive gain in nanowire photodetectors", Appl. Phys. Lett., 99, 143110, 2011
6. Hongsik Park, Roderic Beresford, Ryong Ha, Heon-Jin Choi, Hyunjung Shin, and Jimmy Xu, "Evaluation of metal-nanowire electrical contacts by measuring end-contact resistance", *Nanotechnology* **23** 245201 (2012)
7. Chih-Hsun Hsu and Jimmy Xu, "Diamond Nanowire – a challenge from the extremes", Nanoscale, 2012, 4(17), 5293-5299.
8. S.M. Hollen, J. Shanline, J.M. Xu, J.M. Valles Jr. "Cooper Pair Insulator phase induced in amorphous Pb 0.9Bi0.1 thin films", Physica C 486, 23–25, 2013
9. S. M. Hollen, G. E. Fernandes, J. M. Xu, and J. M. Valles Jr, "Collapse of the Cooper pair phase coherence length at a superconductor to insulator transition", Physical Rev. B, **87**, 054512, 2013
10. S. M. Hollen, J Shainline, J. M. Xu, and J. M. Valles Jr, "Cooper pair insulator phase induced in amorphous PbBi thin films", Physica C: Superconductivity 486, 23-15, 2013
11. Y. Park, Y. Hirose, S. Nakao, T. Fukumura, J. Xu and T. Hasegawa, "Quantum confinement effect in Bi anti-dot thin films with tailored pore wall widths and thicknesses", Appl. Phys. Lett., 104, 023106, 2014.
12. J. C. Joy, X. Zhang, C. Zhao, S. M. Hollen, J. M. Valles Jr, G. Fernandes, and J. M. Xu, "Evolution of the Cooper Pair Insulator Phase in a-Bi Films Grown on Nanohoneycomb Substrates with Varying Surface Topography", Bull. Am. Phys. Soc., 50, 2014
13. S. M. Hollen, G. Fernandes, J. M. Xu, and J. M. Valles, Jr., "Fate of the Bose insulator in the limit of strong localization and low Cooper-pair density in ultrathin films", Phys. Rev. B. 90, 140506, 2014
14. "Magnetic Flux Disorder Impact on the Superconductor to Insulator Transition and its Critical Resistance" (reference number: NPHYS-2015-02-00360), which was recently submitted to Nature Physics.

Papers in Refereed Conferences:

1. SM Hollen, HQ Nguyen, E Rudisaile, J Shainline, G Fernandes, JM Xu, JM Valles, “Cooper pair localization in a-Bi thin films near the superconductor-insulator transition”, APS Meeting Abstract 1, 25005, 2011
2. SM Hollen, HQ Nguyen, E Rudisaile, J Shainline, G Fernandes, JM Xu, JM Valles, “Cooper pair localization in a-Bi thin films near the superconductor-insulator transition”, APS Meeting Abstract 1, 25005, 2011
3. Gustavo Fernandes; Hongsik Park; Jin Ho Kim; Jimmy Xu, “Giant Photoconductivity Gain in Nanowire Photodetectors and the Effect of Photo-Modulation of Contact Injection”, CLEO 2011, pp. 1-2, Baltimore, MD, May 1-6, 2011
4. SM Hollen, JC Joy, AH Berg, G Fernandes, J Shainline, JM Xu, JM Valles, “The extent of the Cooper pair insulator phase in amorphous Pb0. 9Bi0. 1 nanohoneycomb films”, APS Meeting Abstracts 1, 23006, 2012
5. Y. Park, Y. Hirose, S. Nako, T. Fukumura, J. Kim, J. Xu, T. Hasegawa, “Electrical transport properties of porous Bi thin films”, 60th Japanese Society of Applied Physics, Spring Meeting, March 27-30, 2013.
6. J. Valles, S. Hollen, G Fernandes, J.M. Xu, “Observation of the collapse of the Cooper pair phase coherence length at the superconductor to insulator transition”, APS Meeting Abstract 1, 35009, 2013
7. JC Joy, SM Hollen, C Zhao, G Fernandes, JM Xu, JM Valles, “Transport Behavior of Ultrathin Films with NanoThickness Undulations in the Strongly Localized Regime”, APS Meeting Abstracts 1, 35005, 2013
8. J.C. Joy, X. Zhang, S.M. Hollen, C. Zhao, G. Fernandes, J.M. Xu, and J.M. Valles, Jr. , “Evolution of the Cooper Pair Insulator Phase in a-Bi Films Grown on Nanohoneycomb Substrates with Varying Surface Topography”, APS March Meeting, 2014

Invited Talks, Seminars, Colloquia, Plenary & Keynote Speeches, Lectures:

1. Hyunjung Shin and Jimmy Xu, “Synthesis of bismuth nanowires with diameter and length control — An approach for forming band-gap engineered homojunction”, US-Korea 2010 Meeting, Seattle, WA, USA, Aug 10-13, 2010
2. Jimmy Xu, “Nanostructured Materials”, Annual Scientific Congress of Ministry of Higher Education, Science and Technology, Dominican Republic, Santo Domingo, June 14-15, 2012

References:

[1] P. Hongsik, B. Roderic, H. Ryong, C. Heon-Jin, S. Hyunjung, and X. Jimmy, "Evaluation of metal–nanowire electrical contacts by measuring contact end resistance," *Nanotechnology,* vol. 23, p. 245201, 2012.

[2] H. Park, D. Han, J. H. Kim, C.-H. Hsu, H. Shin, and J. Xu, "One Material, Multiple Faces - Nanostructured Bismuth," *ECS Transactions,* vol. 25, pp. 25-33, September 25, 2009 2009.

[3] J. H. Kim, H. Park, C. H. Hsu, and J. Xu, "Facile Synthesis of Bismuth Sulfide Nanostructures and Morphology Tuning by a Biomolecule," *Journal of Physical Chemistry C,* vol. 114, pp. 9634-9639, Jun 3 2010.

[4] H. Park, R. Beresford, S. Hong, and J. Xu, "Geometry- and size-dependence of electrical properties of metal contacts on semiconducting nanowires," *Journal of Applied Physics,* vol. 108, Nov 1 2010.

[5] S. K. Panda, D. Han, H. Yoo, H. Shin, H. Park, and J. Xu, "Synthesis of Step-Shaped Bismuth Nanowires—An Approach Towards the Fabrication of Self-Homojunction," *Electrochemical and Solid-State Letters,* vol. 14, pp. E21-E24, June 1, 2011 2011.

[6] H. Park, J. H. Kim, R. Beresford, and J. Xu, "Effects of electrical contacts on the photoconductive gain of nanowire photodetectors," *Applied Physics Letters,* vol. 99, p. 143110, 2011.

[7] Y. Park, Y. Hirose, S. Nakao, T. Fukumura, J. Xu, and T. Hasegawa, "Quantum confinement effect in Bi anti-dot thin films with tailored pore wall widths and thicknesses," *Applied Physics Letters,* vol. 104, p. 023106, 2014.

[8] S. M. Hollen, G. E. Fernandes, J. M. Xu, and J. M. Valles, "Collapse of the Cooper pair phase coherence length at a superconductor-to-insulator transition," *Physical Review B,* vol. 87, Feb 26 2013.

[9] S. M. Hollen, H. Q. Nguyen, E. Rudisaile, M. D. Stewart, J. Shainline, J. M. Xu*, et al.*, "Cooper-pair insulator phase in superconducting amorphous Bi films induced by nanometer-scale thickness variations," *Physical Review B,* vol. 84, Aug 25 2011.

[10] M. Stewart, H. Nguyen, S. Hollen, A. Yin, J. Xu, and J. Valles, "Enhanced suppression of superconductivity in amorphous films with nano-scale patterning," *Physica C: Superconductivity,* vol. 469, pp. 774-777, 2009.

[11] M. D. Stewart, A. Yin, J. M. Xu, and J. M. Valles, "Superconducting Pair Correlations in an Amorphous Insulating Nanohoneycomb Film," *Science,* vol. 318, pp. 1273-1275, November 23, 2007 2007.

[12] J. J. Tu, C. C. Homes, and M. Strongin, "Optical Properties of Ultrathin Films: Evidence for a Dielectric Anomaly at the Insulator-to-Metal Transition," *Physical Review Letters,* vol. 90, p. 017402, 01/10/ 2003.

[13] H. Kind, H. Yan, B. Messer, M. Law, and P. Yang, "Nanowire Ultraviolet Photodetectors and Optical Switches," *Advanced Materials,* vol. 14, pp. 158-160, 2002.

[14] Y. Gu, J. P. Romankiewicz, J. K. David, J. L. Lensch, and L. J. Lauhon, "Quantitative Measurement of the Electron and Hole Mobility−Lifetime Products in Semiconductor Nanowires," *Nano Letters,* vol. 6, pp. 948-952, 2006/05/01 2006.

[15] A. Armstrong, G. T. Wang, and A. A. Talin, "Depletion-Mode Photoconductivity Study of Deep Levels in GaN Nanowires," *Journal of Electronic Materials,* vol. 38, pp. 484-489, 2009/04/01 2009.

[16] H. Bao, X. Cui, C. M. Li, Y. Gan, J. Zhang, and J. Guo, "Photoswitchable Semiconductor Bismuth Sulfide (Bi2S3) Nanowires and Their Self-Supported Nanowire Arrays," *The Journal of Physical Chemistry C,* vol. 111, pp. 12279-12283, 2007/08/01 2007.

[17] Y. Xi, C. Hu, X. Zhang, Y. Zhang, and Z. L. Wang, "Optical switches based on nanowires synthesized by molten salt solvent method," *Solid State Communications,* vol. 149, pp. 1894-1896, 11// 2009.

[18] C. Soci, A. Zhang, B. Xiang, S. A. Dayeh, D. P. R. Aplin, J. Park*, et al.*, "ZnO Nanowire UV Photodetectors with High Internal Gain," *Nano Letters,* vol. 7, pp. 1003-1009, 2007/04/01 2007.

[19] R. R. Mehta and B. S. Sharma, "Photoconductive gain greater than unity in CdSe films with Schottky barriers at the contacts," *Journal of Applied Physics,* vol. 44, pp. 325-328, 1973.

[20] O. Katz, V. Garber, B. Meyler, G. Bahir, and J. Salzman, "Gain mechanism in GaN Schottky ultraviolet detectors," *Applied Physics Letters,* vol. 79, pp. 1417-1419, 2001.

[21] Y.-F. Lin and W.-B. Jian, "The Impact of Nanocontact on Nanowire Based Nanoelectronics," *Nano Letters,* vol. 8, pp. 3146-3150, 2008/10/08 2008.

[22] W. Gu, H. Choi, and K. Kim, "Universal approach to accurate resistivity measurement for a single nanowire: Theory and application," *Applied Physics Letters,* vol. 89, p. 253102, 2006.

[23] Y.-M. Lin, S. B. Cronin, J. Y. Ying, M. S. Dresselhaus, and J. P. Heremans, "Transport properties of Bi nanowire arrays," *Applied Physics Letters,* vol. 76, pp. 3944-3946, 2000.

[24] Z. Zhang, X. Sun, M. S. Dresselhaus, J. Y. Ying, and J. Heremans, "Electronic transport properties of single-crystal bismuth nanowire arrays," *Physical Review B,* vol. 61, pp. 4850-4861, 02/15/ 2000.

[25] M. E. T. Molares, N. Chtanko, T. W. Cornelius, D. Dobrev, I. Enculescu, R. H. Blick*, et al.*, "Fabrication and contacting of single Bi nanowires," *Nanotechnology,* vol. 15, p. S201, 2004.

[26] W. Shim, J. Ham, K. I. Lee, W. Y. Jeung, M. Johnson, and W. Lee, "On-film formation of bi nanowires with extraordinary electron mobility," *Nano Lett,* vol. 9, pp. 18-22, Jan 2009.

[27] J. Ham, W. Shim, D. H. Kim, K. H. Oh, P. W. Voorhees, and W. Lee, "Watching bismuth nanowires grow," *Applied Physics Letters,* vol. 98, p. 043102, 2011.

[28] W. Shim, J. Ham, J.-S. Noh, and W. Lee, "Structure-dependent growth control in nanowire synthesis via on-film formation of nanowires," *Nanoscale Research Letters,* vol. 6, p. 196, 2011.

[29] Y. Peng, D.-H. Qin, R.-J. Zhou, and H.-L. Li, "Bismuth quantum-wires arrays fabricated by electrodeposition in nanoporous anodic aluminum oxide and its structural properties," *Materials Science and Engineering: B,* vol. 77, pp. 246-249, 9/29/ 2000.

[30] J. Kye Jin, L. Jun Min, L. Eunsongyi, and L. Wooyoung, "Individual Pd nanowire hydrogen sensors fabricated by electron-beam lithography," *Nanotechnology,* vol. 20, p. 135502, 2009.

[31] R. Yan, D. Gargas, and P. Yang, "Nanowire photonics," *Nat Photon,* vol. 3, pp. 569-576, 10//print 2009.

[32] J. Wang, M. S. Gudiksen, X. Duan, Y. Cui, and C. M. Lieber, "Highly Polarized Photoluminescence and Photodetection from Single Indium Phosphide Nanowires," *Science,* vol. 293, pp. 1455-1457, August 24, 2001 2001.

[33] Y. H. Ahn and J. Park, "Efficient visible light detection using individual germanium nanowire field effect transistors," *Applied Physics Letters,* vol. 91, p. 162102, 2007.

[34] MarsiliF, V. B. Verma, J. A. Stern, HarringtonS, A. E. Lita, GerritsT*, et al.*, "Detecting single infrared photons with 93% system efficiency," *Nat Photon,* vol. 7, pp. 210-214, 03//print 2013.

[35] DienstA, M. C. Hoffmann, FaustiD, J. C. Petersen, PyonS, TakayamaT*, et al.*, "Bi-directional ultrafast electric-field gating of interlayer charge transport in a cuprate superconductor," *Nat Photon,* vol. 5, pp. 485-488, 08//print 2011.

[36] U. Welp, K. Kadowaki, and R. Kleiner, "Superconducting emitters of THz radiation," *Nat Photon,* vol. 7, pp. 702-710, 09//print 2013.

[37] K. A. Parendo, L. M. Hernandez, A. Bhattacharya, and A. M. Goldman, "Anomalous parallel-field negative magnetoresistance in ultrathin films near the superconductor-insulator transition," *Physical Review B,* vol. 70, p. 212510, 12/28/ 2004.

[38] H. Q. Nguyen, S. M. Hollen, M. D. Stewart, J. Shainline, A. J. Yin, J. M. Xu*, et al.*, "Observation of Giant Positive Magnetoresistance in a Cooper Pair Insulator," *Physical Review Letters,* vol. 103, Oct 9 2009.

[39] J. Toudert, R. Serna, and M. Jiménez de Castro, "Exploring the Optical Potential of Nano-Bismuth: Tunable Surface Plasmon Resonances in the Near Ultraviolet-to-Near Infrared Range," *The Journal of Physical Chemistry C,* vol. 116, pp. 20530-20539, 2012/09/27 2012.

[40] J. Seidel, "Generation and Detection of THz waves."

[41] X.-C. Zhang and J. Xu, "Generation and Detection of THz Waves," in *Introduction to THz Wave Photonics*, ed: Springer US, 2010, pp. 27-48.

[42] D. Coquillat, S. Nadar, F. Teppe, N. Dyakonova, S. Boubanga-Tombet, W. Knap*, et al.*, "Room temperature detection of sub-terahertz radiation in double-grating-gate transistors," *Optics express,* vol. 18, pp. 6024-6032, 2010.

[43] J. Parashar, S. Chauhan, P. Purohit, and V. Agrawal, "Terahertz surface plasmon excitation over a bismuth thin film by an electron beam," *Journal of Physics and Chemistry of Solids,* vol. 74, pp. 1751-1755, 2013.